Entrance channel effects on sub-barrier capture

R. A. Kuzyakin
Omsk State Transport University, 644046 Omsk, Russia

V. V. Sargsyan, G. G. Adamian, and N. V. Antonenko
Joint Institute for Nuclear Research, 141980 Dubna, Russia

(Received 17 February 2015; revised manuscript received 10 April 2015; published 2 July 2015)

Within the quantum diffusion approach, the capture process of a projectile nucleus by a target nucleus is studied at bombarding energies above and below the Coulomb barrier. The entrance channel effects on the partial and total capture cross sections and the mean angular momentum of the captured system are studied in the reactions leading to ^{156,160}Er, ^{170}Hf, ^{200}Pb, ^{216}Ra, and ^{220}Th compound nuclei.

DOI: 10.1103/PhysRevC.92.014603 PACS number(s): 25.70.Jj, 24.10.−i, 24.60.−k

I. INTRODUCTION

Recently many experimental and theoretical studies have been devoted to investigation of fusion and capture processes at near-barrier and deep sub-barrier energies [1–4]. So far, the study of fusion (capture) was mainly focused on measuring and calculating the excitation function: the fusion (capture) cross section as a function of the energy of colliding nuclei. The fusion (capture) cross section is an integral property of the angular-momentum distribution of partial fusion (capture) cross section. Because similar fusion (capture) cross sections can be obtained with different angular-momentum distributions, the angular-momentum distribution is more sensitive to basic ingredients of the model than the fusion (capture) cross section [5]. For example, in many reactions the fusion (capture) cross sections are described well, but the mean angular momenta are not reproduced [6]. Therefore, a description of experimental angular-momentum distributions of partial fusion (capture) cross sections or their moments is a good test of the viability of fusion (capture) models. It is noteworthy that investigation of partial cross sections is important for better understanding the survival of a compound nucleus in the formation of evaporation residues, especially at high angular momenta, when a significant part of the energy goes to the nucleus rotation.

From all sets of fusion (capture) reactions, those which lead to the same compound nucleus are of great interest [7–14]. In these reactions one can study the entrance channel effects on fusion (capture) cross sections and other characteristics of the process. Such kind of information can be used, for instance, to verify the fusion (capture) models [7,10] and to ascertain the role of quasifission in asymmetric reactions [11–14].

In the present paper the quantum diffusion approach [15–18] is applied to study the entrance channel effects on the total and partial capture cross sections and the mean angular momentum of the captured system in the reactions leading to the compound nuclei ^{156}Er (^{12}C + ^{144}Sm and ^{64}Ni + ^{92}Zr), ^{160}Er (^{16}O + ^{144}Nd, ^{37}Cl + ^{123}Sb, ^{64}Ni + ^{96}Zr, and ^{80}Se + ^{80}Se), ^{170}Hf (^{28}Si + ^{142}Ce, ^{32}S + ^{138}Ba, and ^{48}Ti + ^{122}Sn), ^{200}Pb (^{16}O + ^{184}W), ^{216}Ra (^{12}C + ^{144}Sm, ^{30}Si + ^{186}W, and ^{48}Ca + ^{168}Er), and ^{220}Th (^{16}O + ^{204}Pb, ^{34}S + ^{186}W, ^{50}Ti + ^{170}Er, and ^{96}Zr + ^{124}Sn). The mean angular momentum in question is an important feature of the capture process and affects the angular anisotropy of fission and quasifission products following capture. The formalism used proved to be quite successful in describing the capture process

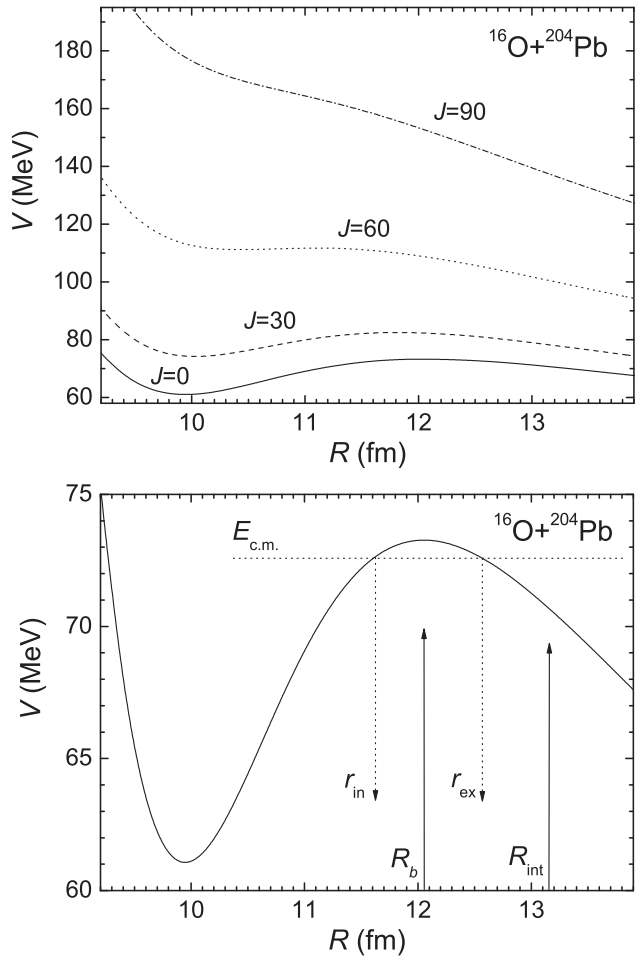

FIG. 1. The nucleus-nucleus potentials calculated at $J = 0$ (solid curve), 30 (dashed curve), 60 (dotted curve), and 90 (dash-dotted curve) for the ^{16}O + ^{204}Pb reaction. The position R_b of the Coulomb barrier, interaction radius $R_{\rm int}$, and external $r_{\rm ex}$ and internal $r_{\rm in}$ turning points for some value of bombarding energy $E_{\rm c.m.}$ are indicated at $J = 0$.

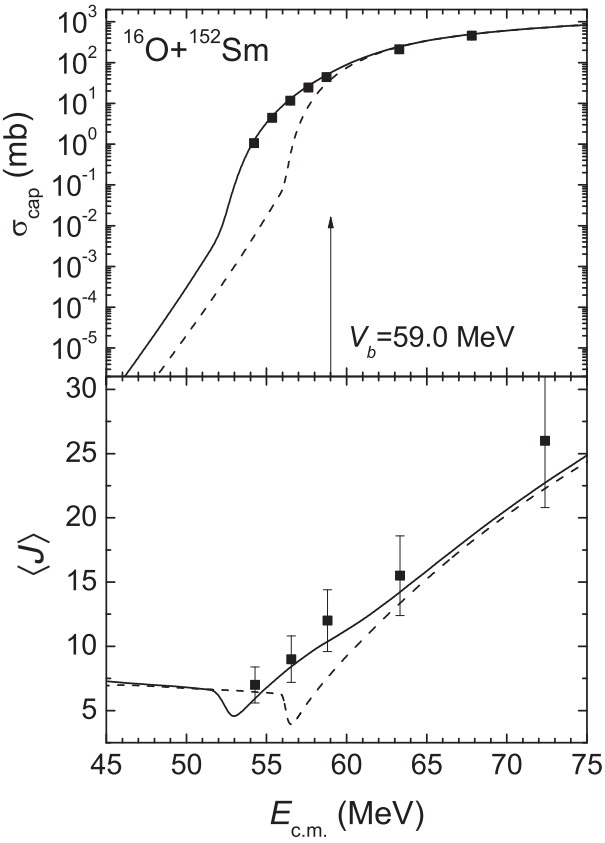

FIG. 2. The calculated capture cross sections σ_{cap} and the mean angular momenta $\langle J \rangle$ of captured system vs $E_{c.m.}$ are compared with the experimental data for the $^{16}O + ^{152}Sm$ reaction. The experimental cross sections are taken from Ref. [33] (closed squares) and the experimental values of $\langle J \rangle$ from Ref. [34] (closed squares). The calculations with and without taking into consideration the deformation effect are shown by solid and dashed lines, respectively. The following quadrupole deformation parameters are used: $\beta_2(^{16}O) = 0$ and $\beta_2(^{152}Sm) = 0.31$ [32]. The height V_b of the Coulomb barrier for the spherical nuclei case is indicated by the arrow.

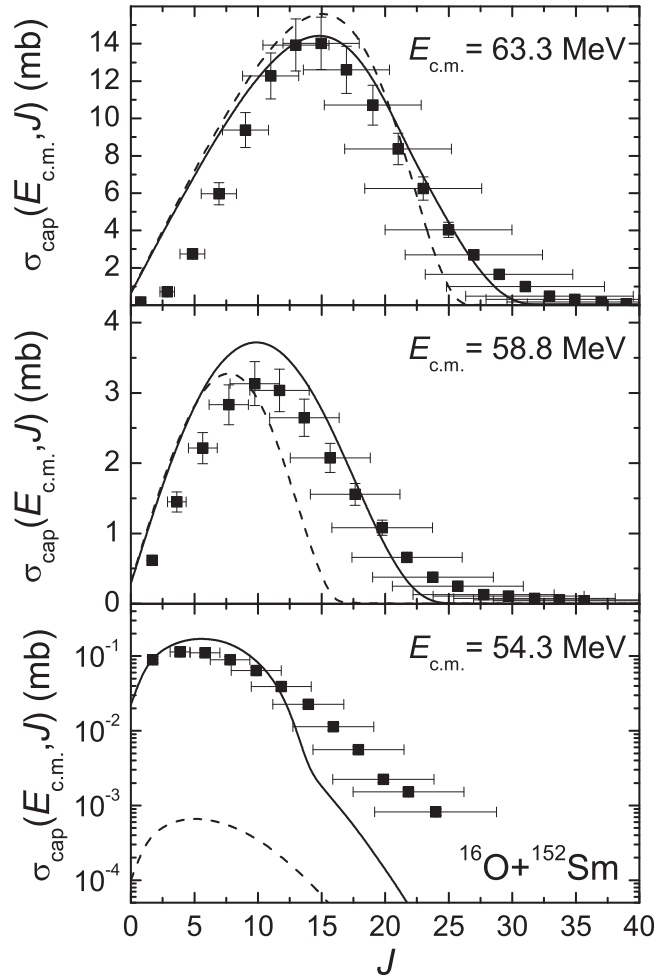

FIG. 3. The calculated partial capture cross sections vs J are compared with the experimental data from Ref. [34] (closed squares) for the $^{16}O + ^{152}Sm$ reaction at indicated $E_{c.m.}$. The calculations with and without taking into consideration the deformation effect are shown by solid and dashed lines, respectively. The following quadrupole deformation parameters are used: $\beta_2(^{16}O) = 0$ and $\beta_2(^{152}Sm) = 0.31$ [32].

at bombarding energies above and well below the Coulomb barrier in a large number of various reactions [15–17,19,20]. Because the details of our theoretical treatment were already published in Refs. [15–17,19–21], the model will be shortly described in Sec. II. The calculated results will be presented in Sec. III. The summary and conclusions will be given in Sec. IV.

II. MODEL

In the quantum diffusion approach the collisions of nuclei are treated in terms of a single collective variable: the relative distance between the colliding nuclei. The nuclear deformation effects are taken into consideration through the dependence of the nucleus-nucleus potential on the deformations and orientations of colliding nuclei. Our approach takes into consideration the fluctuation and dissipation effects in collisions of heavy ions which model the coupling with various channels (for example, coupling of the relative motion with low-lying collective modes such as dynamical quadrupole and octupole modes of target and projectile [22]). We have to mention that many quantum-mechanical and non-Markovian effects accompanying the passage through the potential barrier are taken into consideration in our formalism [15–17,20,21,23,24]. The details of used formalism are presented in our previous articles [15–17]. One should stress that the diffusion model which is including the quantum statistical effects was also proposed in Refs. [25–28].

The capture cross section is a sum of partial capture cross sections [15–17],

$$\sigma_{cap}(E_{c.m.}) = \sum_J \sigma_{cap}(E_{c.m.},J) = \frac{\pi\hbar^2}{2\mu E_{c.m.}} \sum_J (2J+1) \int_0^{\pi/2} d\theta_1 \sin\theta_1 \times \int_0^{\pi/2} d\theta_2 \sin\theta_2 P_{cap}(E_{c.m.},J,\theta_1,\theta_2), \quad (1)$$

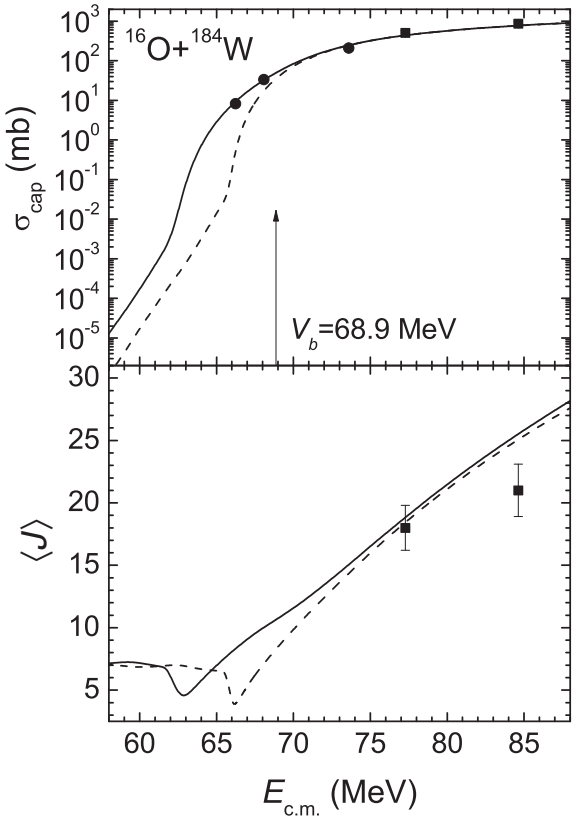

FIG. 4. The same as in Fig. 2, but for the ^{16}O + ^{184}W reaction. The experimental cross sections are taken from Refs. [35] (closed circles) and [36] (closed squares) and the experimental values of $\langle J \rangle$ from Ref. [36] (closed squares). The following quadrupole deformation parameters are used: $\beta_2(^{16}\mathrm{O}) = 0$ and $\beta_2(^{184}\mathrm{W}) = 0.24$ [32].

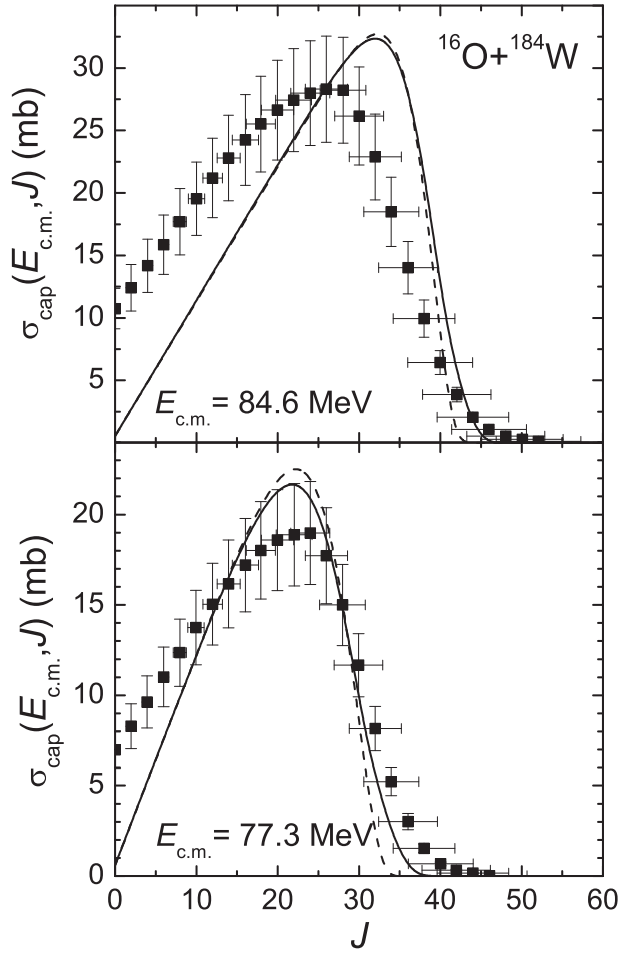

FIG. 5. The calculated partial capture cross sections vs J are compared with the experimental data from Ref. [36] (closed squares) for the ^{16}O + ^{184}W reaction at indicated $E_{c.m.}$. The calculations with and without taking into consideration the deformation effect are shown by solid and dashed lines, respectively. The following quadrupole deformation parameters are used: $\beta_2(^{16}\mathrm{O}) = 0$ and $\beta_2(^{184}\mathrm{W}) = 0.24$ [32].

where $\mu = m_0 A_1 A_2/(A_1 + A_2)$ is the reduced mass [m_0 is the nucleon mass, $A_1 = Z_1 + N_1$ and $A_2 = Z_2 + N_2$ are mass numbers of nuclei, and Z_i and N_i ($i = 1,2$) are the proton and neutron numbers of nuclei], and the summation is over the possible values of angular momentum J at a given bombarding energy $E_{c.m.}$. Knowing the potential of the interacting nuclei for each orientation, one can obtain the partial capture probability P_{cap}, which is defined by the passing probability of the potential barrier in the relative distance R at a given J. The mean angular momentum of the captured system is calculated with the following formula:

$$\langle J \rangle = \frac{1}{\sigma_{cap}(E_{c.m.})} \sum_J J \sigma_{cap}(E_{c.m.}, J). \qquad (2)$$

The value of P_{cap} is obtained by integrating the propagator G from the initial state (R_0, P_0) at time $t = 0$ to the final state (R, P) at time t (P is a momentum):

$$P_{cap} = \lim_{t\to\infty} \int_{-\infty}^{r_{in}} dR \int_{-\infty}^{\infty} dP\, G(R,P,t|R_0,P_0,0)$$
$$= \lim_{t\to\infty} \frac{1}{2} \mathrm{erfc}\left[\frac{-r_{in} + \overline{R(t)}}{\sqrt{\Sigma_{RR}(t)}}\right]. \qquad (3)$$

The second equality in Eq. (3) is obtained by using the propagator $G = \pi^{-1}|\det \Sigma^{-1}|^{1/2} \exp(-\mathbf{v}^T \Sigma^{-1} \mathbf{v})$ ($\mathbf{v}^T = (\mathrm{v}_R, \mathrm{v}_P)$, $\mathrm{v}_R(t) = R - \overline{R(t)}$, $\mathrm{v}_P(t) = P - \overline{P(t)}$, $R_0 = \overline{R(t=0)}$, $P_0 = \overline{P(t=0)}$, $\Sigma_{ij}(t) = 2\overline{\mathrm{v}_i(t)\mathrm{v}_j(t)}$, $\Sigma_{ij}(t=0) = 0$, $i,j = R,P$) calculated in Ref. [29] for an inverted oscillator which approximates the nucleus-nucleus potential V in the variable R. The frequency ω of this oscillator with an internal turning point r_{in} is defined from the condition of equality of the classical actions of approximated and realistic potential barriers of the same height at given J and $E_{c.m.}$ (see Fig. 1). It should be noted that the passage through the Coulomb barrier locally approximated by a parabola was previously studied in Refs. [23,24,26–28]. This approximation is well justified for the reactions and energy range, which are considered here. Finally, one can find the expression for the capture probability:

$$P_{cap} = \frac{1}{2} \mathrm{erfc}\left[\left(\frac{\pi s_1(\gamma - s_1)}{2\mu\hbar(\omega_0^2 - s_1^2)}\right)^{1/2} \frac{\mu\omega_0^2 R_0/s_1 + P_0}{[\gamma \ln(\gamma/s_1)]^{1/2}}\right], \qquad (4)$$

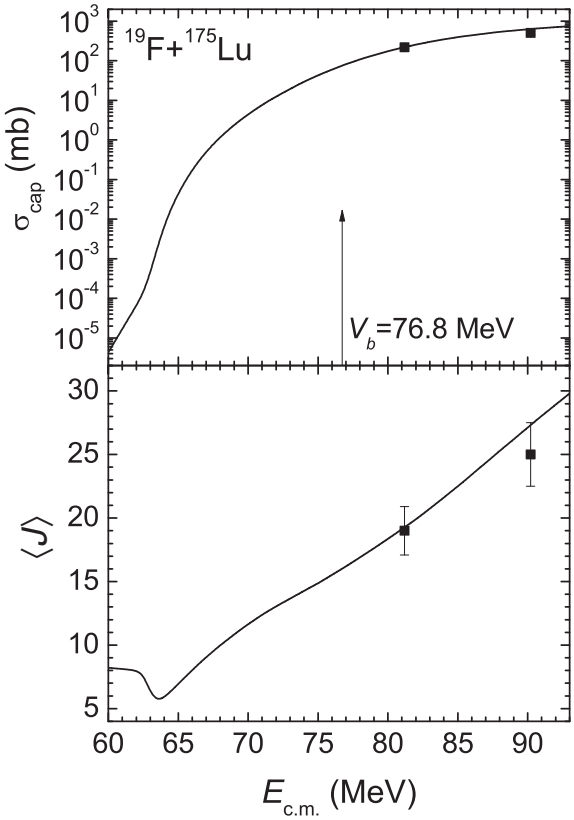

FIG. 6. The calculated capture cross sections σ_{cap} and the mean angular momenta $\langle J \rangle$ of captured system vs $E_{c.m.}$ are compared with the experimental data from Ref. [37] (closed circles) for the ^{19}F + ^{175}Lu reaction. The following quadrupole deformation parameters are used: $\beta_2(^{21}\text{F}) = 0.56$ and $\beta_2(^{173}\text{Lu}) = 0.33$. The height V_b of the Coulomb barrier for the spherical nuclei case is indicated by the arrow.

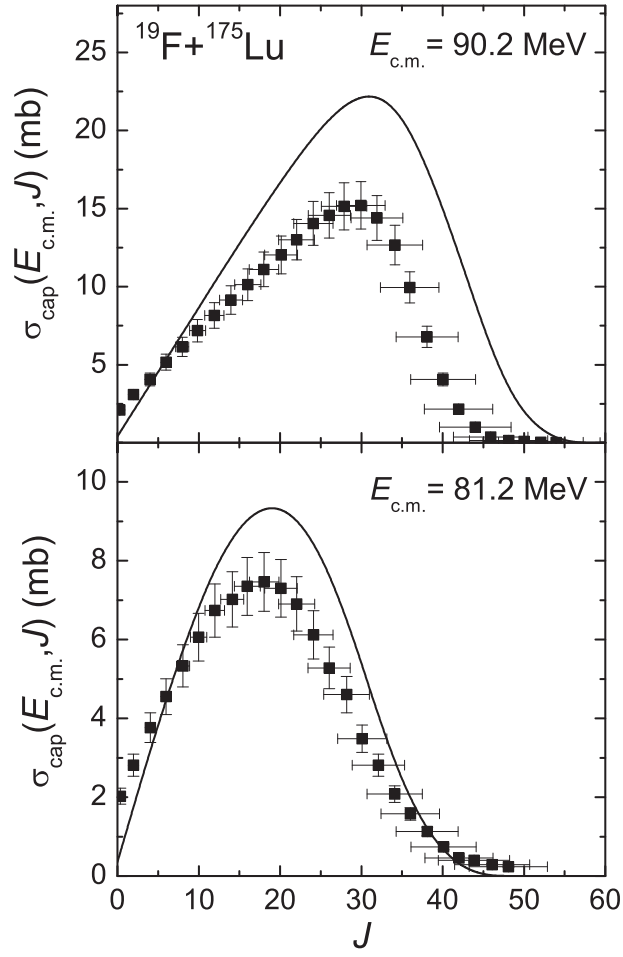

FIG. 7. The calculated partial capture cross sections vs J for the ^{19}F + ^{175}Lu reaction at indicated $E_{c.m.}$ are compared with the experimental data from Ref. [37] (closed squares) for evaporation residue cross sections. The following quadrupole deformation parameters are used: $\beta_2(^{21}\text{F}) = 0.56$ and $\beta_2(^{173}\text{Lu}) = 0.33$.

where γ is the internal-excitation width, $\omega_0^2 = \omega^2\{1 - \hbar\tilde{\lambda}\gamma/[\mu(s_1+\gamma)(s_2+\gamma)]\}$ is the renormalized frequency in the Markovian limit, and the value of $\tilde{\lambda}$ is related to the strength of linear coupling in coordinate between collective and internal subsystems. The s_i are the real roots ($s_1 \geqslant 0 > s_2 \geqslant s_3$) of the following equation:

$$(s+\gamma)\left(s^2 - \omega_0^2\right) + \hbar\tilde{\lambda}\gamma s/\mu = 0. \quad (5)$$

The details of the used formalism are presented in Refs. [15,17]. We have to mention that most of the quantum-mechanical, dissipative effects and non-Markovian effects accompanying the passage through the potential barrier are taken into consideration in our formalism [15,17,23]. For example, the non-Markovian effects appear in the calculations through the internal-excitation width γ.

As shown in Refs. [15–17], the nuclear forces start to play a role at $R_{\text{int}} = R_b + 1.1$ fm where the nucleon density of colliding nuclei approximately reaches 10% of the saturation density. If the value of r_{ex} corresponding to the external turning point is larger than the interaction radius R_{int}, we take $R_0 = r_{\text{ex}}$ and $P_0 = 0$ in Eq. (4) (see Fig. 1). For $r_{\text{ex}} < R_{\text{int}}$, it is natural to start our treatment with $R_0 = R_{\text{int}}$ and P_0 is defined by the kinetic energy at $R = R_0$. In this case the friction hinders the classical motion to proceed toward smaller values of R. If $P_0 = 0$ at $R_0 > R_{\text{int}}$, the friction almost does not play a role in the transition through the barrier. Thus, two regimes of interaction at sub-barrier energies differ by the action of the nuclear forces and the role of friction at $R = r_{\text{ex}}$.

In addition to the parameters related to the nucleus-nucleus potential, two parameters $\hbar\gamma = 15$ MeV and the friction coefficient $\hbar\lambda = -\hbar(s_1 + s_2) = 2$ MeV are used for calculating the capture probability. The value of coupling strength $\tilde{\lambda}$ is set to obtain this value of $\hbar\lambda$. The most realistic friction coefficients in the range of $\hbar\lambda_R \approx 1$–2 MeV are suggested from the study of deep inelastic and fusion reactions [30]. These values are close to those calculated within the mean-field approach [31]. All calculated results presented are obtained with the same set of parameters and are rather insensitive to a reasonable variation of them [15–17,23,24]. All parameters of the model are set as in Ref. [15]. The heights of the calculated Coulomb barriers $V_b = V(R_b)$ (R_b is the position of the Coulomb

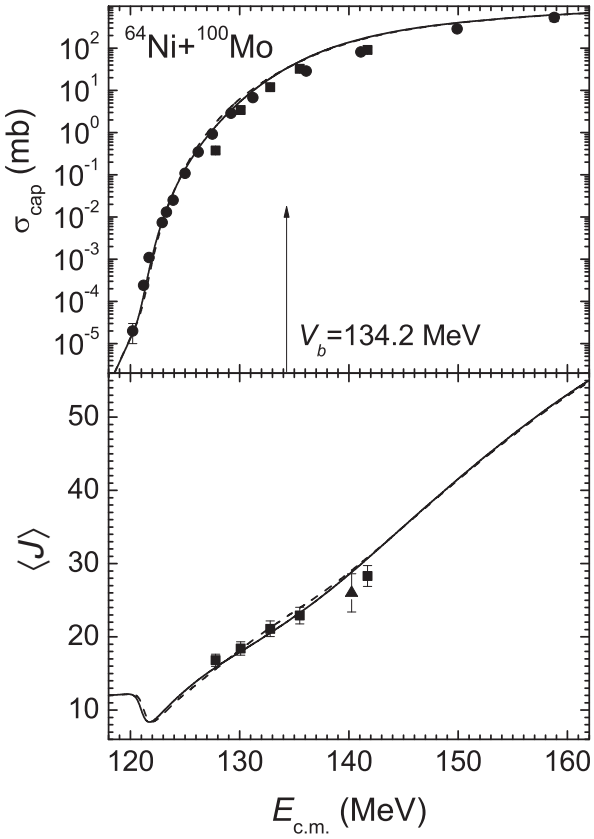

FIG. 8. The calculated capture cross sections σ_{cap} and the mean angular momenta $\langle J \rangle$ of captured system vs $E_{c.m.}$ are compared with the experimental data for the ^{64}Ni + ^{100}Mo reaction. The experimental cross sections are taken from Refs. [38] (closed squares) and [39] (closed circles) and the experimental values of $\langle J \rangle$ from Refs. [38] (closed squares) and [40] (closed triangles). The calculations with and without taking into consideration the neutron transfer process are shown by solid and dashed lines, respectively. The following quadrupole deformation parameters are used: $\beta_2(^{64}\text{Ni}) = 0.09$, $\beta_2(^{66}\text{Ni}) = 0.16$ [32], $\beta_2(^{98}\text{Mo}) = 0.17$ [32], and $\beta_2(^{100}\text{Mo}) = 0.23$ [32]. The height V_b of the Coulomb barrier for the spherical nuclei case is indicated by the arrow.

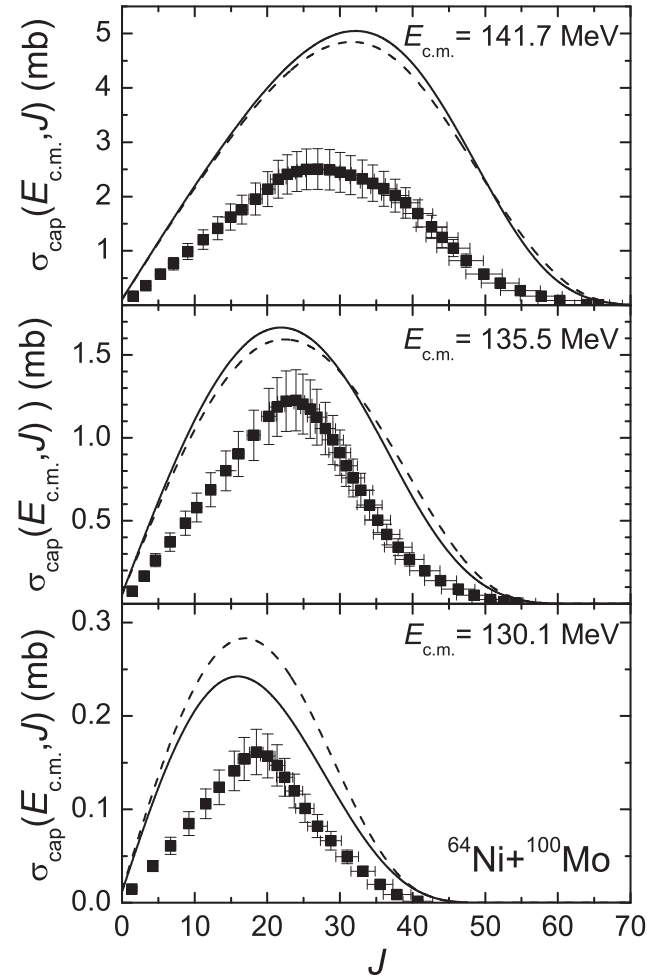

FIG. 9. The calculated partial capture cross sections vs J are compared with the experimental data from Ref. [38] (closed squares) for the ^{64}Ni + ^{100}Mo reaction at indicated $E_{c.m.}$. The calculations with and without taking into consideration the neutron transfer process are shown by solid and dashed lines, respectively. The following quadrupole deformation parameters are used: $\beta_2(^{64}\text{Ni}) = 0.09$, $\beta_2(^{66}\text{Ni}) = 0.16$ [32], $\beta_2(^{98}\text{Mo}) = 0.17$ [32], and $\beta_2(^{100}\text{Mo}) = 0.23$ [32].

barrier) are adjusted to the experimental data for the fusion or capture cross sections. To calculate the nucleus-nucleus interaction potential $V(R)$, we use the procedure presented in Refs. [15–17]. For the nuclear part of the nucleus-nucleus potential, the double-folding formalism with the Skyrme-type density-dependent effective nucleon-nucleon interaction is used.

The considered nuclei are proposed to be spherical or deformed with the quadrupole deformation parameters β_2. The quadrupole deformation parameters are taken from Ref. [32] for the deformed even-even nuclei. In Ref. [32] the quadrupole deformation parameters β_2 are given for the first excited 2^+ states of nuclei. For the nuclei deformed in the ground state, the β_2 in 2^+ state is similar to the β_2 in the ground state and we use β_2 from Ref. [32] in the calculations. For the deformed nuclei with odd atomic numbers β_2 are chosen to be equal to the maximum deformation parameter of the neighboring even nuclei with the same number of neutrons [$\beta_2 = 0.17, 0.33$, and 0.28 for the nuclei ^{123}Sb, ^{173}Lu, and ^{179}Ta, respectively] [32]. For double-magic and almost all semimagic nuclei, in the ground state we take $\beta_2 = 0$ and 0.05, respectively. Because there are uncertainties in the definition of the values of ground state β_2 in light- and medium-mass nuclei, we use the values of the quadrupole deformation parameter $\beta_2 = -0.3$, 0.09, and 0 for the nuclei ^{12}C, ^{64}Ni, and ^{90}Zr, respectively, extracted in Ref. [16] from the comparison of the calculated capture cross sections with the experimental data for other reactions.

Following the hypothesis of Ref. [16], we assume that the sub-barrier capture mainly depends on the two-neutron transfer with the positive Q_{2n} value. Our assumption is that, before the projectile is captured by the target nucleus (before

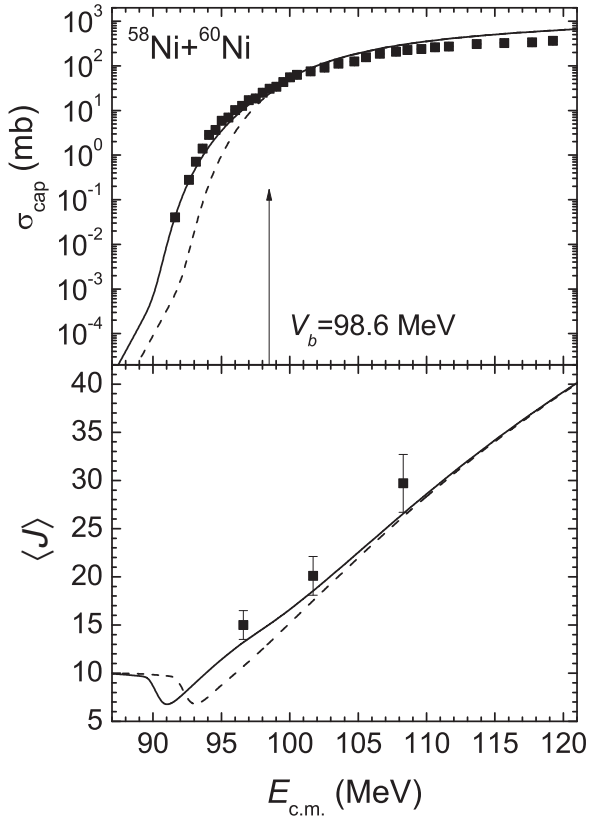

FIG. 10. The calculated capture cross sections σ_{cap} and the mean angular momenta $\langle J \rangle$ of captured system vs $E_{c.m.}$ are compared with the experimental data in the evaporation residue channel for the ^{58}Ni + ^{60}Ni reaction. The calculations with and without consideration of transfer are shown by solid and dashed lines, respectively. The experimental cross sections σ_{cap} are taken from Ref. [41] (closed squares) and the experimental values of $\langle J \rangle$ from Ref. [42] (closed squares). The following quadrupole deformation parameters are used: $\beta_2(^{58}\text{Ni}) = 0.05$, $\beta_2(^{60}\text{Ni}) = 0.21$ [32]. The height V_b of the Coulomb barrier for the spherical nuclei case is indicated by the arrow.

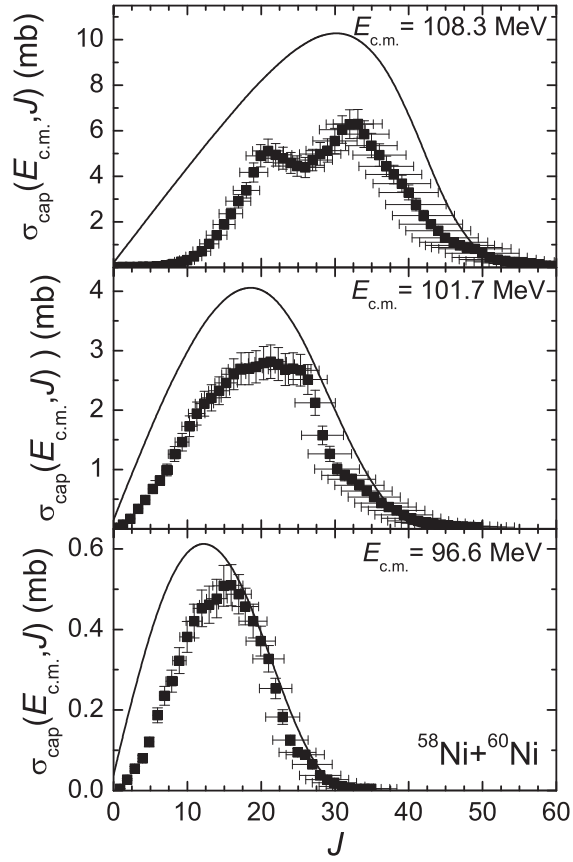

FIG. 11. The calculated partial capture cross sections vs J are compared with the experimental data from Ref. [42] (closed squares) in evaporation residue channel for the ^{58}Ni + ^{60}Ni reaction at indicated $E_{c.m.}$. The following quadrupole deformation parameters are used: $\beta_2(^{58}\text{Ni}) = 0.05$, $\beta_2(^{60}\text{Ni}) = 0.21$ [32].

the crossing of the Coulomb barrier), which is the slow process, the two-neutron transfer occurs at larger separations that can lead to the population of the first 2^+ state in the recipient nucleus. In the calculations, for such excited recipient nuclei we use the experimental deformation parameters β_2 related to the first 2^+ states from the table of Ref. [32]. For nuclei with odd atomic numbers β_2 of the first 2^+ state are chosen to be equal to the maximum deformation parameter of the first 2^+ state of the neighboring even nuclei with the same number of neutrons. We assume that after two-neutron transfer the residues of donor nuclei remain in the ground state with corresponding quadrupole deformation. Because after two-neutron transfer, the mass numbers, the deformation parameters of interacting nuclei, and, respectively, the height and shape of the Coulomb barrier are changed, one can expect the enhancement, weak influence, or suppression of the capture [16,18].

III. CALCULATED RESULTS

A. Effect of quadrupole deformation in the entrance channel

In Figs. 2–5 the calculated partial and total capture cross sections and mean angular momenta of captured system for the reactions $^{16}\text{O} + ^{152}\text{Sm}$ and $^{16}\text{O} + ^{184}\text{W}$ are in good agreement with available experimental data [33–36]. It is seen that a good agreement between calculated results and experimental data is observed only when the deformation of colliding nuclei is taken into account, particular at small $E_{c.m.}$. With nuclei deformation effect the right-hand side (relatively to the maximum) of partial distribution is cut under larger J values (Figs. 3 and 5). Such a behavior is more pronounced with decreasing bombarding energy. As a result, the enhancement of the total capture cross sections is observed at sub-barrier energies.

As seen from Figs. 2 and 4, the nuclei deformation leads to small increase of mean angular momentum. There is a minimum in the dependence of $\langle J \rangle$ on $E_{c.m.}$ which is related to the change of the regime of interaction between colliding nuclei [15]. The position of this minimum is shifted to smaller energies, its depth decreases, and the width becomes larger,

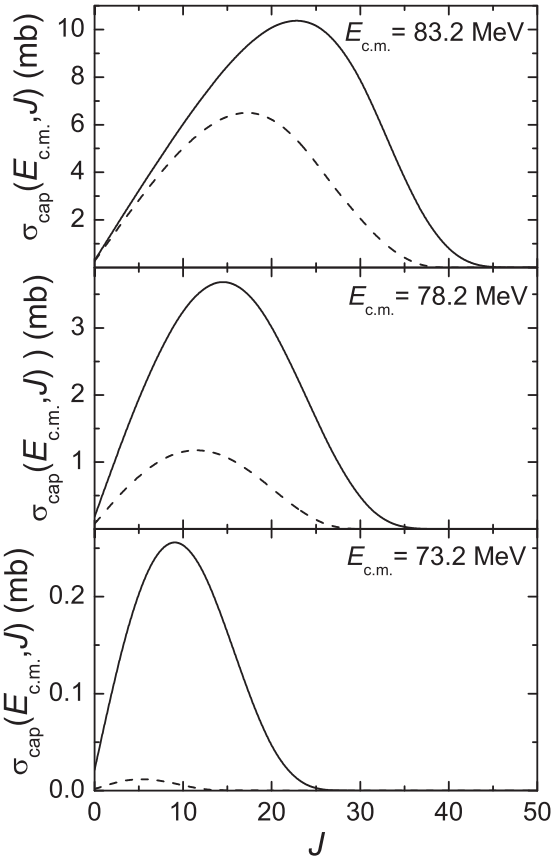

FIG. 12. The calculated partial capture cross sections vs J for the reactions $^{32}S + {}^{94}Zr$ (solid lines) and $^{32}S + {}^{90}Zr$ (dashed lines) at indicated $E_{c.m.}$. The following quadrupole deformation parameters are used: $\beta_2(^{32}S) = 0.31$ [32], $\beta_2(^{34}S) = 0.25$ [32], $\beta_2(^{90}Zr) = 0$, and $\beta_2(^{92}Zr) = 0.1$ [32].

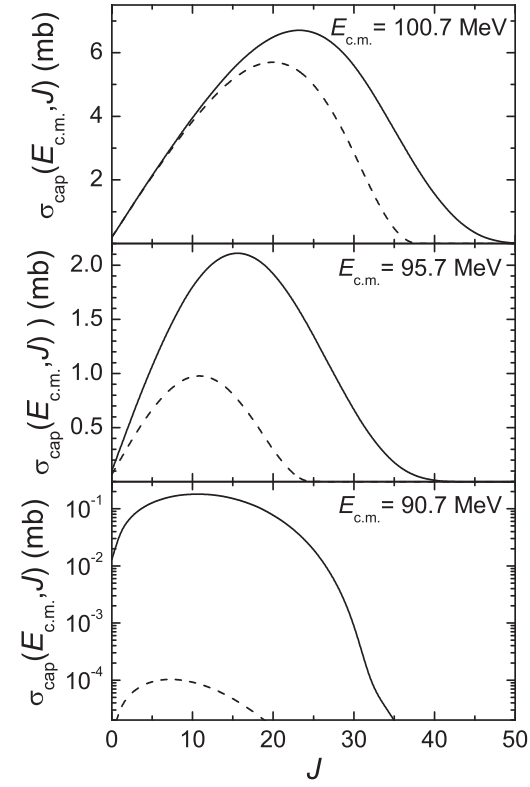

FIG. 13. The calculated partial capture cross sections vs J for the reactions $^{40}Ca + {}^{94}Zr$ (solid lines) and $^{40}Ca + {}^{90}Zr$ (dashed lines) at indicated $E_{c.m.}$. The following quadrupole deformation parameters are used: $\beta_2(^{40}Ca) = 0$, $\beta_2(^{42}Ca) = 0.25$ [32], $\beta_2(^{90}Zr) = 0$, and $\beta_2(^{92}Zr) = 0.1$ [32].

i.e., the minimum becomes less pronounced. On the left-hand side of this minimum the dependence of $\langle J \rangle$ on $E_{c.m.}$ and β_2 is rather weak. The difference between spherical and deformed cases are particularly visible in sub-barrier region (see Figs. 2 and 4). With increasing deformation of nuclei the deviation from the calculated results for spherical nuclei becomes larger. In deeply sub-barrier collisions the value of $\langle J \rangle$ is 5–10. Note that the change in $\langle J \rangle$ behavior, which is related to the deformation of the colliding nuclei, would affect the angular anisotropy of the products of fission-like fragments following capture.

B. Effect of neutron transfer in the entrance channel

In Figs. 6–9 the calculated partial and total capture cross sections and mean angular momenta of captured system for the reactions $^{19}F + {}^{175}Lu \rightarrow {}^{21}F + {}^{173}Lu$ ($Q_{2n} = 0.3$ MeV) and $^{64}Ni + {}^{100}Mo \rightarrow {}^{66}Ni + {}^{98}Mo$ ($Q_{2n} = 0.8$ MeV) (reactions with positive Q_{2n} values) are in good agreement with available experimental data [37–40]. For some reactions the experimental data contain only evaporation residue channels, but not fusion-fission and quasifission channels, so for these reactions the above Coulomb barrier experimental data are lower than the calculated results. Since the contributions of fusion-fission and quasifission channels increase with $E_{c.m.}$ above the Coulomb barrier, the difference between the theoretical results and experimental data must increase with bombarding energy.

One can see in Figs. 8 and 9 that for the $^{64}Ni + {}^{100}Mo$ reaction the neutron transfer process weakly influences the partial and, correspondingly, the total cross sections. This happens because the whole deformation of nuclei system (the nucleus-nucleus interaction) almost do not change after transfer. For the $^{64}Ni + {}^{100}Mo$ reaction, there is the following change of quadrupole deformation parameters: $^{64}Ni(\beta_2 = 0.09) + {}^{100}Mo(\beta_2 = 0.23) \rightarrow {}^{66}Ni(\beta_2 = 0.16) + {}^{98}Mo(\beta_2 = 0.17)$. One can find the reactions with positive two-neutron transfer Q values where the transfer suppresses the capture process [16,18]. This happens if the whole deformation of nucleus system decreases after transfer.

In the case of the $^{58}Ni + {}^{60}Ni$ reaction [41,42] (Figs. 10 and 11), the two-neutron transfer leads to the population of the first 2^+ state in the recipient nucleus: $^{58}Ni(\beta_2 = 0.05) + {}^{60}Ni(\beta_2 = 0.1) \rightarrow {}^{60}Ni(\beta_2 = 0.21) + {}^{58}Ni(\beta_2 = 0.05)$. Due to an increase in the deformation of the recipient nucleus, an enhancement of the partial capture cross section occurs at sub-barrier energies. Because for the $^{58}Ni + {}^{60}Ni$ reaction the experimental data contain only evaporation residue channel, but not fusion-fission and quasifission channels, a

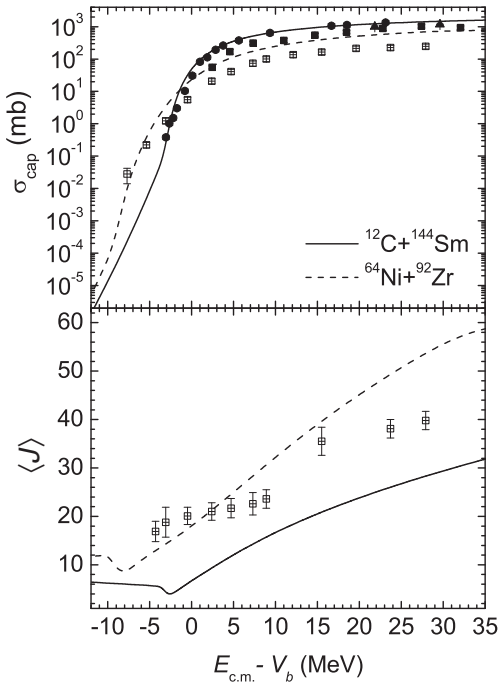

FIG. 14. The calculated capture cross sections σ_{cap} and the mean angular momenta $\langle J \rangle$ of captured system vs $E_{c.m.} - V_b$ are compared with the experimental data for the reactions $^{12}C + {}^{144}Sm$ and $^{64}Ni + {}^{92}Zr$ (compound nucleus ^{156}Er). The experimental cross sections for the $^{12}C + {}^{144}Sm$ reaction are taken from Refs. [44] (closed triangles), [45] (closed squares), and [46] (closed circles) and for the $^{64}Ni + {}^{92}Zr$ from Ref. [43] (open squares). The experimental values of $\langle J \rangle$ for the $^{64}Ni + {}^{92}Zr$ reaction are from Ref. [43] (open squares). The heights V_b of the Coulomb barriers in the case of the spherical nuclei are 46.0 and 129.9 MeV, respectively. The following quadrupole deformation parameters are used: $\beta_2(^{12}C) = -0.3$, $\beta_2(^{144}Sm) = 0.05$, $\beta_2(^{64}Ni) = 0.09$, and $\beta_2(^{92}Zr) = 0.1$ [32].

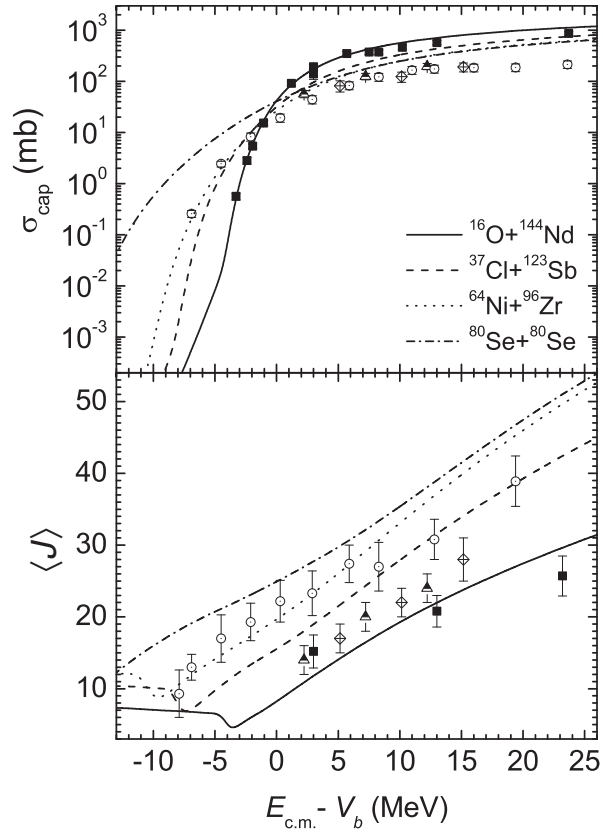

FIG. 15. The same as in Fig. 14, but for the reactions $^{16}O + {}^{144}Nd$, $^{37}Cl + {}^{123}Sb$, $^{64}Ni + {}^{96}Zr$, and $^{80}Se + {}^{80}Se$ (compound nucleus ^{160}Er). The experimental cross sections and mean angular momenta for the $^{16}O + {}^{144}Nd$ reaction are taken from Ref. [47] (squares), for the $^{37}Cl + {}^{123}Sb$ from Ref. [7] (triangles), for the $^{64}Ni + {}^{96}Zr$ from Ref. [43] (circles), and for the $^{80}Se + {}^{80}Se$ from Ref. [7] (rhombuses). The heights V_b of the Coulomb barriers in the case of the spherical nuclei are 57.3, 101.2, 128.5, and 132.8 MeV, respectively. The following quadrupole deformation parameters are used: $\beta_2(^{16}O) = 0$, $\beta_2(^{144}Nd) = 0.12$ [32], $\beta_2(^{37}Cl) = 0.05$, $\beta_2(^{123}Sb) = 0.17$, $\beta_2(^{66}Ni) = 0.16$ [32], $\beta_2(^{94}Zr) = 0.09$ [32], and $\beta_2(^{80}Se) = 0.23$ [32].

good agreement between the experimental and theoretical partial cross sections takes place only for sub-barrier and near barrier energies.

In Figs. 12 and 13 the calculated partial capture cross sections and mean angular momenta of captured system are presented for the reactions $^{32}S + {}^{90}Zr$ ($Q_{2n} < 0$), $^{32}S + {}^{94}Zr$ ($Q_{2n} > 0$), $^{40}Ca + {}^{90}Zr$ ($Q_{2n} < 0$), and $^{40}Ca + {}^{94}Zr$ ($Q_{2n} > 0$). As seen, the difference between the reactions $^{32}S + {}^{90}Zr$ and $^{32}S + {}^{94}Zr$ in the population of the states with large J is smaller than between the reactions $^{40}Ca + {}^{90}Zr$ and $^{40}Ca + {}^{94}Zr$. This difference is explained by the two-neutron transfer process. In the $^{32}S(\beta_2 = 0.31) + {}^{90}Zr(\beta_2 = 0)$ reaction the ^{32}S nucleus is well deformed, and in the $^{32}S(\beta_2 = 0.31) + {}^{94}Zr(\beta_2 = 0.09) \rightarrow {}^{34}S(\beta_2 = 0.25) + {}^{92}Zr(\beta_2 = 0.1)$ ($Q_{2n} = 5.1$ MeV) reaction after two-neutron transfer the final ^{34}S nucleus is also deformed. In contrast, in the $^{40}Ca(\beta_2 = 0) + {}^{90}Zr(\beta_2 = 0)$ reaction the ^{40}Ca nucleus is spherical, and in the $^{40}Ca(\beta_2 = 0) + {}^{94}Zr(\beta_2 = 0.09) \rightarrow {}^{42}Ca(\beta_2 = 0.25) + {}^{92}Zr(\beta_2 = 0.1)$ ($Q_{2n} = 4.9$ MeV) reaction after two-neutron transfer the final ^{42}Ca nucleus is already deformed. So, the change of the nucleus deformation in $^{40}Ca + {}^{94}Zr$ reaction causes the difference between ^{32}S and ^{40}Ca induced reactions.

C. Effect of mass (charge) asymmetry in the entrance channel

To analyze the entrance channel effects of the nuclei reactions, it is helpful to use the mass asymmetry

$$\eta = \frac{A_2 - A_1}{A_2 + A_1} \tag{6}$$

or charge asymmetry

$$\eta_Z = \frac{Z_2 - Z_1}{Z_2 + Z_1} \tag{7}$$

coordinate. In Figs. 14–18 the calculated capture cross sections and mean angular momenta of captured system for the reactions $^{12}C + {}^{144}Sm$ and $^{64}Ni + {}^{92}Zr$ (compound nucleus

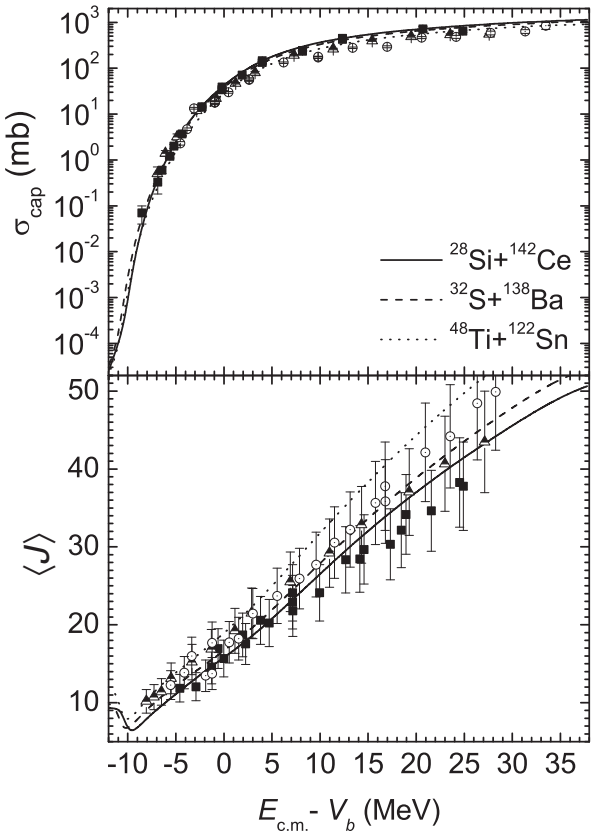

FIG. 16. The same as in Fig. 14, but for the reactions ^{28}Si + ^{142}Ce, ^{32}S + ^{138}Ba, and ^{48}Ti + ^{122}Sn (compound nucleus ^{170}Hf). The experimental cross sections for the reactions ^{28}Si + ^{142}Ce (squares), ^{32}S + ^{138}Ba (triangles), and ^{48}Ti + ^{122}Sn (circles) are taken from Ref. [10]. The experimental values of $\langle J \rangle$ for the reactions ^{28}Si + ^{142}Ce (squares), ^{32}S + ^{138}Ba (triangles), and ^{48}Ti + ^{122}Sn (circles) are taken from Ref. [48]. The heights V_b of the Coulomb barriers in the case of the spherical nuclei are 96.0, 106.1, and 125.9 MeV, respectively. The following quadrupole deformation parameters are used: $\beta_2(^{30}\text{Si}) = 0.32$ [32], $\beta_2(^{140}\text{Ce}) = 0.11$ [32], $\beta_2(^{34}\text{S}) = 0.25$ [32], $\beta_2(^{136}\text{Ba}) = 0.13$ [32], $\beta_2(^{50}\text{Ti}) = 0.17$ [32], and $\beta_2(^{120}\text{Sn}) = 0.11$ [32].

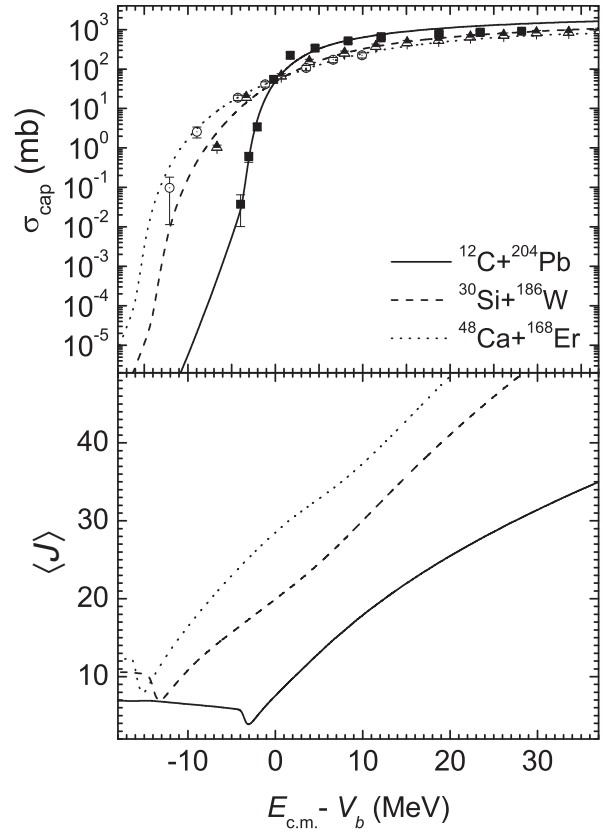

FIG. 17. The same as in Fig. 14, but for the reactions ^{12}C + ^{204}Pb, ^{30}Si + ^{186}W, and ^{48}Ca + ^{168}Er (compound nucleus ^{216}Ra). The experimental cross sections for the reactions ^{12}C + ^{204}Pb (squares), ^{30}Si + ^{186}W (triangles), and ^{48}Ca + ^{168}Er (circles) are taken from Ref. [11]. The heights V_b of the Coulomb barriers in the case of the spherical nuclei are 56.7, 115.7, and 151.2 MeV, respectively. The following quadrupole deformation parameters are used: $\beta_2(^{12}\text{C}) = -0.3$, $\beta_2(^{204}\text{Pb}) = 0$, $\beta_2(^{32}\text{Si}) = 0.22$ [32], $\beta_2(^{184}\text{W}) = 0.24$ [32], $\beta_2(^{48}\text{Ca}) = 0$, and $\beta_2(^{168}\text{Er}) = 0.34$ [32].

^{156}Er), ^{16}O + ^{144}Nd, ^{37}Cl + ^{123}Sb, ^{64}Ni + ^{96}Zr, and ^{80}Se + ^{80}Se (compound nucleus ^{160}Er), ^{28}Si + ^{142}Ce, ^{32}S + ^{138}Ba, and ^{48}Ti + ^{122}Sn (compound nucleus ^{170}Hf), ^{12}C + ^{144}Sm, ^{30}Si + ^{186}W, and ^{48}Ca + ^{168}Er (compound nucleus ^{216}Ra), and ^{16}O + ^{204}Pb, ^{34}S + ^{186}W, ^{50}Ti + ^{170}Er, and ^{96}Zr + ^{124}Sn (compound nucleus ^{220}Th) are presented. The calculated results are in rather good agreement with the available experimental data [43–50]. As seen, the decrease of the reaction asymmetry leads to larger values of capture cross section at above barrier energies and to smaller values of capture cross section at below barrier energies. At the Coulomb barrier the cross sections are close for the reactions leading to the same compound nucleus. At the same time the mean angular momenta of captured systems are larger for more symmetric cases at above barrier and below barrier energies almost in all reactions. The position of the minimum in $\langle J \rangle$ dependence shifts to smaller energies relatively to the barriers with the decreasing asymmetry in the entrance channel. This minimum is originated because of the change of the regime of interaction between the colliding nuclei [15]. At energies above the Coulomb barrier, the small deviations between the calculated σ_{cap} and $\langle J \rangle$ and corresponding experimental data probably arise from the fact that the fusion-fission and quasifission channels are not in the experimental capture cross sections.

One can see in Fig. 18 that the ^{96}Zr + ^{124}Sn reaction is out of the trend shown in Figs. 15 and 17 where the sub-barrier capture growths with decreasing asymmetry in the entrance channel. For more asymmetric reactions ^{34}S + ^{186}W and ^{50}Ti + ^{170}Er, the capture cross sections are larger at sub-barrier energies. Also in the ^{50}Ti + ^{170}Er reaction the mean angular momentum exceeds the value for the ^{96}Zr + ^{124}Sn reaction at $E_{\text{c.m.}} - V_b < 10$ MeV. The reason for such a behavior is larger deformations in ^{34}S + ^{186}W and ^{50}Ti + ^{170}Er systems after two-neutron transfer compared to the ^{96}Zr + ^{124}Sn

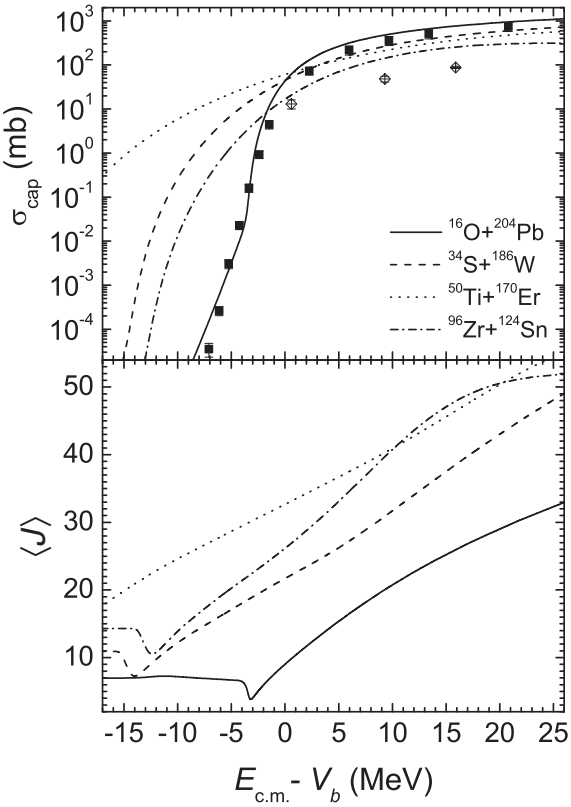

FIG. 18. The same as in Fig. 14, but for the reactions ^{16}O + ^{204}Pb, ^{34}S + ^{186}W, ^{50}Ti + ^{170}Er, and ^{96}Zr + ^{124}Sn (compound nucleus ^{220}Th). The experimental cross sections for the ^{16}O + ^{204}Pb reaction are taken from Ref. [49] (squares) and for the ^{96}Zr + ^{124}Sn from Ref. [50] (rhombuses). The heights V_b of the Coulomb barriers in the case of the spherical nuclei are 73.6, 131.4, 165.5, and 199.2 MeV, respectively. The following quadrupole deformation parameters are used: $\beta_2(^{16}\mathrm{O}) = 0$, $\beta_2(^{204}\mathrm{Pb}) = 0$, $\beta_2(^{36}\mathrm{S}) = 0.17$ [32], $\beta_2(^{184}\mathrm{W}) = 0.24$ [32], $\beta_2(^{52}\mathrm{Ti}) = 0.27$, $\beta_2(^{168}\mathrm{Er}) = 0.34$ [32], $\beta_2(^{96}\mathrm{Zr}) = 0.08$ [32], and $\beta_2(^{124}\mathrm{Sn}) = 0.1$ [32].

system. The larger deformations of colliding nuclei result in the enhancement of the capture cross sections and mean angular momenta at near and sub-barrier energies [16,18]. Therefore, the ^{96}Zr + ^{124}Sn reaction with stiff nuclei is out of the trends observed in the reactions with soft nuclei.

In Fig. 19 the calculated partial capture cross sections for the reactions ^{16}O + ^{144}Nd and ^{64}Ni + ^{96}Zr (compound nucleus ^{160}Er) at different bombarding energies are compared with the available experimental data [47,51]. Some overestimation of the experimental data is probably related to the fact that the fusion-fission and quasifission channels are disregarded in the corresponding measurements, and there are only the data for the evaporation residue channel. In Fig. 19 the maximum of the partial distribution becomes smaller with decreasing reaction asymmetry and its position shifts to large values of J. This shift is found to be larger with increasing $E_{\mathrm{c.m.}} - V_b$. The decrease of the reaction asymmetry leads to the broader partial distribution, and its right-hand side becomes less steep.

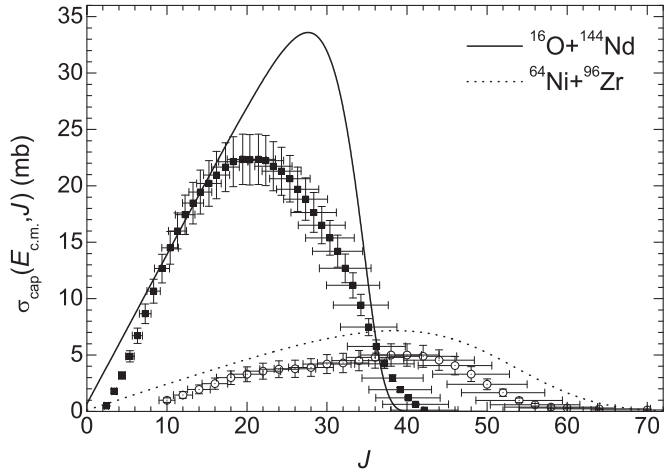

FIG. 19. The calculated partial capture cross sections versus J are compared with the experimental data for the reactions ^{16}O + ^{144}Nd at $E_{\mathrm{c.m.}} - V_b = 13$ MeV and ^{64}Ni + ^{96}Zr at $E_{\mathrm{c.m.}} - V_b = 11$ MeV (compound nucleus ^{160}Er). The experimental partial evaporation residue cross sections for the ^{16}O + ^{144}Nd reaction are taken from Ref. [47] (squares) and for the ^{64}Ni + ^{96}Zr from Ref. [51] (circles). The heights V_b of the Coulomb barriers in the case of the spherical nuclei are 57.3 MeV and 128.5 MeV, respectively. The following quadrupole deformation parameters are used: $\beta_2(^{16}\mathrm{O}) = 0$, $\beta_2(^{144}\mathrm{Nd})$=0.12 [32], $\beta_2(^{66}\mathrm{Ni})$=0.16 [32], and $\beta_2(^{94}\mathrm{Zr})$=0.09 [32].

In Figs. 20 and 21 the calculated capture cross sections and the mean angular momenta of captured system versus η are presented for the reactions ^{16}O + ^{144}Nd ($\eta = 0.8$), ^{37}Cl + ^{123}Sb ($\eta = 0.54$), ^{64}Ni + ^{96}Zr ($\eta = 0.2$), and ^{80}Se + ^{80}Se ($\eta = 0$) (compound nucleus ^{160}Er) and for the reactions ^{16}O + ^{204}Pb ($\eta = 0.86$), ^{34}S + ^{186}W ($\eta = 0.69$), ^{50}Ti + ^{170}Er ($\eta = 0.55$), and ^{96}Zr + ^{124}Sn ($\eta = 0.13$) (compound nucleus ^{220}Th) at different values of $E_{\mathrm{c.m.}} - V_b$. For ^{160}Er compound nucleus (see Fig. 20), we have the following: at above barrier energies the capture cross section grows with reaction asymmetry, at barrier energies it is almost constant, and at energies below barrier it dramatically falls down. The mean angular momentum almost linearly decreases with increasing η at all energies. For ^{220}Th compound nucleus (see Fig. 2), we have the same picture for all reactions except ^{96}Zr + ^{124}Sn ($\eta = 0.13$). As mentioned above, the reason of such a behavior is larger deformations in the systems ^{34}S + ^{186}W and ^{50}Ti + ^{170}Er after two-neutron transfer as compared to the ^{96}Zr + ^{124}Sn system.

IV. SUMMARY

By using the quantum diffusion approach, we systematically studied the deformation and neutron transfer effects in the partial capture cross sections and in the mean angular momentum of the captured system in various reactions. The calculated results are in rather good agreement with the available experimental data. The deformation effect in the entrance channel is important at energies below the Coulomb barrier. When disregarding this effect one cannot describe the partial cross sections and, correspondingly,

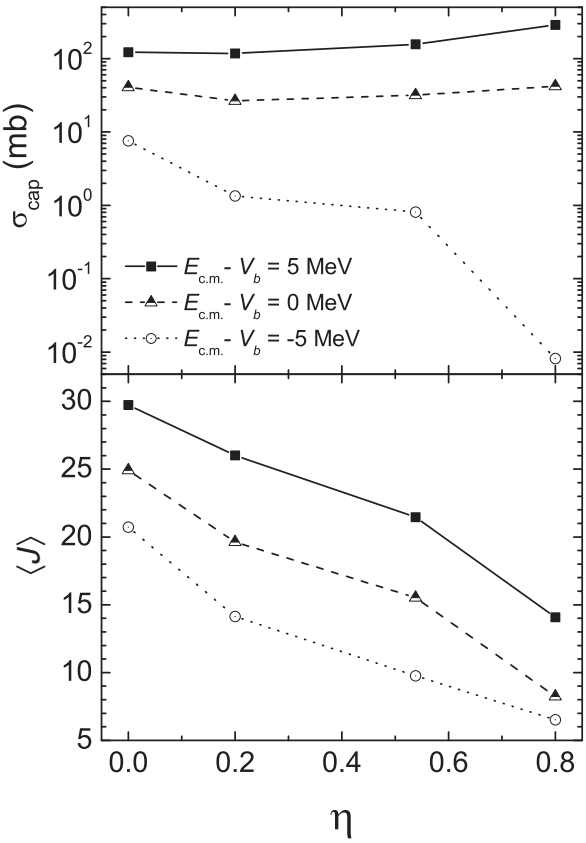

FIG. 20. The calculated capture cross sections σ_{cap} and the mean angular momenta $\langle J \rangle$ of captured system (lower part) versus η for the reactions ^{16}O + ^{144}Nd ($\eta = 0.8$), ^{37}Cl + ^{123}Sb ($\eta = 0.538$), ^{64}Ni + ^{96}Zr ($\eta = 0.2$), and ^{80}Se + ^{80}Se ($\eta = 0$) (compound nucleus ^{160}Er) at indicated values of $E_{c.m.} - V_b$. The heights V_b of the Coulomb barriers in the case of the spherical nuclei are 57.3 MeV, 101.2 MeV, 128.5 MeV, and 132.8 MeV, respectively. The following quadrupole deformation parameters are used: $\beta_2(^{16}\text{O}) = 0$, $\beta_2(^{144}\text{Nd}) = 0.12$ [32], $\beta_2(^{37}\text{Cl}) = 0.05$, $\beta_2(^{123}\text{Sb}) = 0.17$, $\beta_2(^{66}\text{Ni}) = 0.16$ [32], $\beta_2(^{94}\text{Zr}) = 0.09$ [32], and $\beta_2(^{80}\text{Se}) = 0.23$ [32].

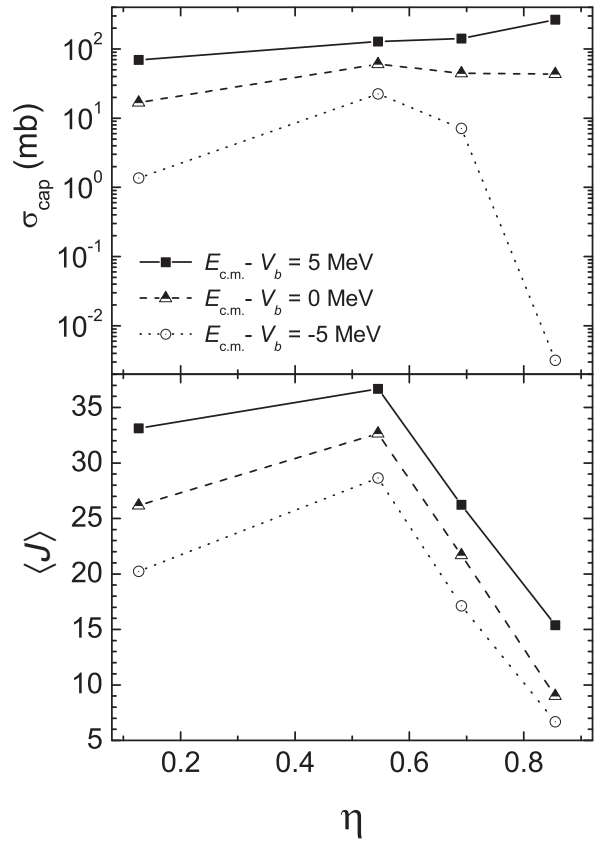

FIG. 21. The same as in Fig. 20, but for the reactions ^{16}O + ^{204}Pb ($\eta = 0.855$), ^{34}S + ^{186}W ($\eta = 0.691$), ^{50}Ti + ^{170}Er ($\eta = 0.545$), and ^{96}Zr + ^{124}Sn ($\eta = 0.127$) (compound nucleus ^{220}Th). The heights V_b of the Coulomb barriers in the case of the spherical nuclei are 73.6 MeV, 131.4 MeV, 165.5 MeV, and 199.2 MeV, respectively. The following quadrupole deformation parameters are used: $\beta_2(^{16}\text{O}) = 0$, $\beta_2(^{204}\text{Pb}) = 0$, $\beta_2(^{36}\text{S}) = 0.17$ [32], $\beta_2(^{184}\text{W}) = 0.24$ [32], $\beta_2(^{52}\text{Ti}) = 0.27$, $\beta_2(^{168}\text{Er}) = 0.34$ [32], $\beta_2(^{96}\text{Zr}) = 0.08$ [32], and $\beta_2(^{124}\text{Sn}) = 0.1$ [32].

the total capture cross sections. At $E_{c.m.} > V_b$ the role of deformation effect becomes minor. The neutron transfer ($Q_{2n} > 0$) influences the sub-barrier capture if it results in the change of the deformations of the reaction partners. The sub-barrier fusion is indifferent to the neutron transfer if either $Q_{2n} < 0$ or the nucleus-nucleus interaction potential is not changed by the neutron transfer as in the reactions with stiff nuclei.

The entrance channel mass (charge) asymmetry effect was studied in the capture cross section and in the mean angular momentum of the captured system in the reactions leading to ^{156,160}Er, ^{170}Hf, ^{216}Ra, and ^{220}Th compound nuclei. Almost in all reactions considered the decrease of the reaction asymmetry leads to larger values of capture cross section at above-barrier energies and to smaller values of capture cross section at below-barrier energies. At the Coulomb barrier the cross sections are close for the reactions leading to the same compound nucleus. Some general trends on the mass asymmetry are revealed if the reactions with soft deformed nuclei are considered. The mean angular momenta of captured systems are larger for more symmetric reactions at energies above and below barrier. The reactions with stiff nuclei deviate from these trends.

Thus, all entrance channel effects like the deformations, neutron transfer, and mass (charge) asymmetry effects have to be taken into consideration for describing capture (fusion) reactions.

ACKNOWLEDGMENT

This work was supported by RFBR and JINR grants. The IN2P3(France)-JINR(Dubna) Cooperation Program is gratefully acknowledged.

[1] B. B. Back, H. Esbensen, C. L. Jiang, and K. E. Rehm, Rev. Mod. Phys. **86**, 317 (2014) and references therein.

[2] C. Simenel, Eur. Phys. J. A **48**, 152 (2012) and references therein.

[3] N. Keeley, R. Raabe, N. Alamanos, and J. L. Sida, Prog. Part. Nucl. Phys. **59**, 579 (2007) and references therein.

[4] L. F. Canto, P. R. S. Gomes, R. Donangelo, and M. S. Hussein, Phys. Rep. **424**, 1 (2006) and references therein.

[5] G. Giardina, F. Hanappe, A. I. Muminov, A. K. Nasirov, and L. Stuttge, Nucl. Phys. A **671**, 165 (2000); G. Fazio *et al.*, Phys. Rev. C **72**, 064614 (2005); A. K. Nasirov, G. Mandaglio, M. Manganaro, A. I. Muminov, G. Fazio, and G. G. Giardina, Phys. Lett. B **686**, 72 (2010); H. Q. Zhang *et al.*, Phys. Rev. C **82**, 054609 (2010).

[6] R. Vandenbosh, Ann. Rev. Nucl. Part. Sci. **42**, 447 (1992).

[7] B. Haas *et al.*, Phys. Rev. Lett. **54**, 398 (1985).

[8] A. Ruckelshausen *et al.*, Phys. Rev. Lett. **56**, 2356 (1986).

[9] S. Gil *et al.*, Phys. Rev. Lett. **65**, 3100 (1990).

[10] S. Gil *et al.*, Phys. Rev. C **51**, 1336 (1995).

[11] R. N. Sagaidak *et al.*, Phys. Rev. C **68**, 014603 (2003).

[12] M. Trotta *et al.*, Nucl. Phys. A **734**, 245 (2004).

[13] R. G. Thomas *et al.*, Phys. Rev. C **77**, 034610 (2008).

[14] G. Mohanto *et al.*, Nucl. Phys. A **890**, 62 (2012).

[15] V. V. Sargsyan, G. G. Adamian, N. V. Antonenko, and W. Scheid, Eur. Phys. J. A **45**, 125 (2010).

[16] V. V. Sargsyan, G. G. Adamian, N. V. Antonenko, W. Scheid, and H. Q. Zhang, Phys. Rev. C **84**, 064614 (2011); **85**, 024616 (2012).

[17] R. A. Kuzyakin, V. V. Sargsyan, G. G. Adamian, N. V. Antonenko, E. E. Saperstein, and S. V. Tolokonnikov, Phys. Rev. C **85**, 034612 (2012); R. A. Kuzyakin, V. V. Sargsyan, G. G. Adamian, and N. V. Antonenko, Phys. Atom. Nucl. **75**, 439 (2012).

[18] R. A. Kuzyakin, V. V. Sargsyan, G. G. Adamian, and N. V. Antonenko, Phys. Atom. Nucl. **76**, 716 (2013).

[19] V. V. Sargsyan, G. G. Adamian, N. V. Antonenko, W. Scheid, and H. Q. Zhang, Phys. Rev. C **91**, 014613 (2015); A. A. Ogloblin *et al.*, Eur. Phys. J. A **50**, 157 (2014).

[20] A. S. Zubov, V. V. Sargsyan, G. G. Adamian, and N. V. Antonenko, Phys. Rev. C **84**, 044320 (2011).

[21] A. S. Zubov, V. V. Sargsyan, G. G. Adamian, N. V. Antonenko, and W. Scheid, Phys. Rev. C **81**, 024607 (2010); **82**, 034610 (2010).

[22] S. Ayik, B. Yilmaz, and D. Lacroix, Phys. Rev. C **81**, 034605 (2010).

[23] V. V. Sargsyan, Z. Kanokov, G. G. Adamian, N. V. Antonenko, and W. Scheid, Phys. Rev. C **80**, 034606 (2009); **80**, 047603 (2009); V. V. Sargsyan, Z. Kanokov, G. G. Adamian, and N. V. Antonenko, Phys. Part. Nucl. **41**, 175 (2010).

[24] Z. Kanokov, Yu. V. Palchikov, G. G. Adamian, N. V. Antonenko, and W. Scheid, Phys. Rev. E **71**, 016121 (2005); Yu. V. Palchikov, Z. Kanokov, G. G. Adamian, N. V. Antonenko, and W. Scheid, *ibid.* **71**, 016122 (2005); R. A. Kuzyakin, V. V. Sargsyan, G. G. Adamian, and N. V. Antonenko, Phys. Rev. A **83**, 062117 (2011); **84**, 032117 (2011).

[25] A. Diaz-Torres, Phys. Rev. C **81**, 041603(R) (2010); **82**, 054617 (2010).

[26] G. Hupin and D. Lacroix, Phys. Rev. C **81**, 014609 (2010).

[27] H. Hofmann, Phys. Rept. **284**, 137 (1997); C. Rummel and H. Hofmann, Nucl. Phys. A **727**, 24 (2003).

[28] N. Takigawa, S. Ayik, K. Washiyama, and S. Kimura, Phys. Rev. C **69**, 054605 (2004).

[29] V. V. Dodonov and V. I. Man'ko, Trudy Fiz. Inst. AN **167**, 7 (1986).

[30] G. G. Adamian, A. K. Nasirov, N. V. Antonenko, and R. V. Jolos, Phys. Part. Nucl. **25**, 583 (1994).

[31] K. Washiyama, D. Lacroix, and S. Ayik, Phys. Rev. C **79**, 024609 (2009); S. Ayik, K. Washiyama, and D. Lacroix, *ibid.* **79**, 054606 (2009).

[32] S. Raman, C. W. Nestor Jr., and P. Tikkanen, At. Data Nucl. Data Tables **78**, 1 (2001).

[33] R. G. Stokstad, Y. Eisen, S. Kaplanis, D. Pelte, U. Smilansky, and I. Tserruya, Phys. Rev. C **21**, 2427 (1980).

[34] A. H. Wuosmaa *et al.*, Phys. Lett. B **263**, 23 (1991).

[35] J. R. Leigh *et al.*, J. Phys. G **14**, L55 (1988).

[36] P. D. Shidling *et al.*, Phys. Rev. C **74**, 064603 (2006).

[37] S. K. Hui *et al.*, Phys. Rev. C **62**, 054604 (2000).

[38] M. L. Halbert *et al.*, Phys. Rev. C **40**, 2558 (1989).

[39] C. L. Jiang *et al.*, Phys. Rev. C **71**, 044613 (2005).

[40] D. Ackermann *et al.*, Nucl. Phys. A **630**, 442 (1998).

[41] A. M. Stefanini *et al.*, Phys. Rev. Lett. **74**, 864 (1995).

[42] S. Courtin *et al.*, Nucl. Phys. A **724**, 125 (2003).

[43] A. M. Stefanini *et al.*, Nucl. Phys. A **548**, 453 (1992).

[44] R. Kossakowski *et al.*, Phys. Rev. C **32**, 1612 (1985).

[45] R. V. F. Janssens *et al.*, Phys. Lett. B **181**, 16 (1986).

[46] D. Abriola *et al.*, Phys. Rev. C **46**, 244 (1992).

[47] G. Duchêne *et al.*, Phys. Rev. C **47**, 2043 (1993).

[48] A. Charlop *et al.*, Phys. Rev. C **49**, R1235 (1994).

[49] M. Dasgupta, D. J. Hinde, A. Diaz-Torres, B. Bouriquet, C. I. Low, G. J. Milburn, and J. O. Newton, Phys. Rev. Lett. **99**, 192701 (2007).

[50] A. M. Vinodkumar *et al.*, Phys. Rev. C **74**, 064612 (2006).

[51] A. M. Stefanini *et al.*, Nucl. Phys. A **538**, 195c (1992).